E3S Web of Conferences **9**, 04007 (2016) DOI: 10.1051/e3sconf/20160904007
E-UNSAT 2016

Two-phase flow effects on the CO_2 injection pressure evolution and implications for the caprock geomechanical stability

Víctor Vilarrasa[1,a], Jesús Carrera[2] and Sebastià Olivella[3]

[1]*École Polytechnique Fédérale de Lausanne, 1015 Lausanne, Switzerland*
[2]*GHS, Institute of Environmental Assessment and Water Research (IDAEA), CSIC, 08034 Barcelona, Spain*
[3]*Dept Geotechnical Engineering and Geosciences, Technical University of Catalonia (UPC-BarcelonaTech), 08034 Barcelona, Spain*

Abstract. Geologic carbon storage is considered to be one of the main solutions to significantly reduce CO_2 emissions to the atmosphere to mitigate climate change. CO_2 injection in deep geological formations entails a two-phase flow, being CO_2 the non-wetting phase. One of the main concerns of geologic carbon storage is whether the overpressure induced by CO_2 injection may compromise the caprock integrity and faults stability. We numerically investigate the two-phase flow effects that govern the overpressure evolution generated by CO_2 injection and how this overpressure affects the caprock geomechanical stability. We find that fluid pressure increases sharply at the beginning of injection because CO_2 has to displace the brine that fills the pores around the injection well, which reduces the relative permeability. However, overpressure decreases subsequently because once CO_2 fills the pores around the injection well, CO_2 can flow easily due to its low viscosity and because the relative permeability to CO_2 increases. Furthermore, the pressure drop that occurs in the capillary fringe due to two-phase flow interference decreases as the CO_2 plume becomes larger. This overpressure evolution induced by CO_2 injection, which remains practically constant with time after the initial peak, is very beneficial for maintaining caprock stability. Thus, the sealing capacity of the caprock will be maintained, preventing CO_2 leakage to occur across the caprock.

1 Introduction

Despite the known necessity to significantly reduce atmospheric carbon dioxide (CO_2) concentration, CO_2 emissions continue increasing worldwide. The rate of increase is such that climate models predict a rise in the mean temperature of the Earth that may have very negative effects on the environment. Governments are aware of these potential negative effects and have recently reached an agreement at the COP21 meeting in Paris to take the necessary measures to avoid a temperature increase higher than 2 °C with respect to the pre-industrial temperature. According to the International Energy Agency (IEA), to achieve such objective, CO_2 emissions should be reduced by more than half with respect to the current CO_2 emissions by 2050 [1]. Furthermore, the IEA considers that geologic carbon storage should contribute with one fifth of the total reduction, which represents storing around 8 Gt of CO_2 per year in deep geological formations by 2050. Currently, only a few Mt of CO_2 are stored each year, mainly in pilot test sites [2, 3]. Thus, a tremendous amount of work has to be done before geologic carbon storage can become a real solution.

Geologic carbon storage consists in capturing CO_2 from point sources, such as industries or hydrocarbon based power plants, transporting the captured CO_2 to the injection well and finally injecting CO_2 in deep saline formations, where it will be permanently kept away from the atmosphere. CO_2 forms a plume around the injection well, displacing the formation brine laterally [4, 5]. CO_2 is the non-wetting phase and is partially miscible in brine [6]. Brine with dissolved CO_2 is denser than brine without dissolved CO_2, which leads to convection cells that enhance CO_2 dissolution [7-9], leading to safer storage. Furthermore, CO_2 is a very compressible fluid: it is a gas in the atmosphere, but at pressures greater than 7.38 MPa and temperatures above 31.04 °C CO_2 becomes a supercritical fluid. The transition to a supercritical fluid usually occurs at a depth of around 800 m [4]. CO_2 will be stored in sedimentary formations deeper than this depth because the high density of supercritical CO_2 makes the storage efficient in terms of volume. Still, supercritical CO_2 is lighter than the resident brine and thus, it tends to float. For this reason, a low-permeability and high entry pressure rock, known as caprock, overlying the storage formation, is required. This caprock provides a hydrodynamic trap for CO_2 that prevents CO_2 from migrating upwards (Figure 1). Apart from a liquid-like density, supercritical CO_2 has a low gas-like dynamic viscosity, which is around one order of magnitude lower than that of brine. Therefore, CO_2 flows more easily than brine. Furthermore, CO_2 injection generates overpressure, reducing the effective stresses, which induces deformations and brings the stress state closer to failure conditions.

[a] Corresponding author: victor.vilarrasariano@epfl.ch

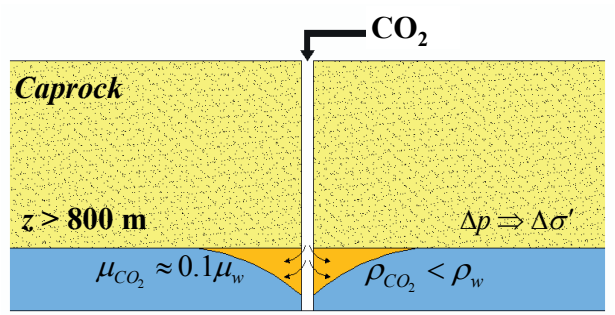

Figure 1. Schematic representation of geologic carbon storage.

One of the main concerns of geologic carbon storage is whether the caprock sealing capacity and faults stability will be maintained [10]. Since CO_2 tends to migrate upwards due to buoyancy, maintaining the caprock sealing capacity is crucial to avoid CO_2 leakage [11]. Nevertheless, sedimentary basins usually present sequences of permeable formations alternated with low permeable rocks that may act as secondary caprocks [12]. In such cases, CO_2 trapping in secondary caprocks would hinder CO_2 from reaching freshwater aquifers or the surface even though leakage occurred across the primary caprock. On the other hand, maintaining fault stability is important to avoid inducing felt seismic events [13]. Even though fault reactivation will not lead to CO_2 leakage [14, 15], it may induce earthquakes that may be felt by the local population. Felt seismicity induced by fluid injection in deep geological formations has led to the closure of several geo-energy related projects (e.g., a geothermal project at Basel, Switzerland [16], the seasonal gas storage project of Castor, Spain [17] and a wastewater disposal project at Guy-Greenbrier, Arkansas [18]). Thus, felt induced seismicity should be avoided to achieve a successful deployment of geological carbon storage.

To predict the geomechanical response of rocks, first, the fluid pressure distribution and evolution needs to be known. Overpressure evolution is well known in single phase flow, presenting a linear buildup with the logarithm of time. However, overpressure becomes more complex both in space and time for two-phase flow, like in CO_2 injection in deep saline formations. Despite this complexity, several studies have aimed at developing analytical solutions of overpressure. Fluid pressure evolution was calculated analytically by Mathias et al. [19] based on the analytical solution of Nordbotten et al. [20] for the CO_2 plume position. Vilarrasa et al. [21] also derived the fluid pressure evolution resulting from the analytical solutions for the CO_2 plume position of Nordbotten et al. [20] and Dentz and Tartakovsky [22], and incorporated a correction in these solutions to account for CO_2 compressibility. In all cases, fluid pressure was predicted to monotonically build up with time as a result of CO_2 injection at a constant mass flow rate. However, a semi-analytical solution that made more realistic assumptions yielded a fluid pressure evolution that peaks shortly after the beginning of injection, but that slightly decreases subsequently [23]. This semi-analytical solution accounts for the buoyancy of CO_2 within the injection well, which leads to (*i*) a CO_2 plume that may not reach the bottom of the storage formation and (*ii*) a CO_2 injection rate that is not uniformly distributed along the whole thickness of the injection well. To validate these analytical and semi-analytical solutions, CO_2 injection in the field is needed.

The experience with overpressure evolution in CO_2 injection sites is quite limited. However, a few pilot tests have already performed CO_2 injection. For example, at Ketzin, Germany, CO_2 pressure underwent a sharp increase at the beginning of injection, but it became practically constant shortly afterwards [24]. Thus, overpressure evolution in the field is more similar to that predicted by the semi-analytical solution of Vilarrasa et al. [23] than to that derived from other analytical solutions. Numerical solutions also predict the sharp increase in injection pressure at the beginning of injection followed by a progressive pressure drop [25-29]. Nevertheless, little attention has been paid to understand the driving mechanisms of overpressure evolution induced by CO_2 injection.

The objective of this paper is to numerically investigate how overpressure evolves when injecting CO_2 in deep saline formations and to analyze how this injection affects to caprock stability. In the following section, we explain the numerical model and capillary properties that we use. Next, we explain how injection pressure evolves when CO_2 is injected through a vertical well. Then, we present the geomechanical implications of overpressure on the caprock integrity. Finally, we summarize and draw the conclusions of this study.

2 Methods

CO_2 injection in deep geological formations is a two-phase flow problem that requires solving the mass conservation of each fluid phase [30]

$$\frac{\partial(\varphi S_\alpha \rho_\alpha)}{\partial t} + \nabla \cdot (\rho_\alpha \mathbf{q}_\alpha) = r_\alpha, \qquad \alpha = c, w \tag{1}$$

where φ [L^3 L^{-3}] is porosity, S_α [-] is saturation of the α-phase, ρ_α [M L^{-3}] is density of the α-phase, t [T] is time, $\mathbf{q}_\alpha$ [L^3 L^{-2} T^{-1}] is the volumetric flux, r_α [M L^{-3} T^{-1}] is the phase change term, i.e., CO_2 dissolution into water and water evaporation into CO_2, and α is either CO_2-rich phase, c, or aqueous phase, w.

Momentum conservation for the fluid phases is expressed using Darcy's law

$$\mathbf{q}_\alpha = -\frac{k k_{r\alpha}}{\mu_\alpha}(\nabla p_\alpha + \rho_\alpha g \nabla z), \qquad \alpha = c, w, \tag{2}$$

where k [L^2] is intrinsic permeability, $k_{r\alpha}$ [-] is the α-phase relative permeability, μ_α [M L^{-1} T^{-1}] is the α-phase viscosity, p_α [M L^{-1} T^{-2}] is the α-phase pressure and g [L T^{-2}] is gravity.

To account for geomechanics, the momentum balance of the solid phase has to be solved. Neglecting inertial terms, it reduces to the equilibrium of stresses

$$\nabla \cdot \boldsymbol{\sigma} + \mathbf{b} = \mathbf{0}, \quad (3)$$

where $\boldsymbol{\sigma}$ [M L^{-1} T^{-2}] is the stress tensor and $\mathbf{b}$ [M L^{-2} T^{-2}] is the body forces vector. The stress-strain relationship, assuming elasticity, is given by Hooke's law

$$\boldsymbol{\varepsilon} = \frac{\sigma'_m}{3K}\mathbf{I} + \frac{1}{2G}\left(\boldsymbol{\sigma}' - \sigma'_m \mathbf{I}\right), \quad (4)$$

where $\boldsymbol{\varepsilon}$ [-] is the elastic strain tensor, $\boldsymbol{\sigma}'$ [M L^{-1} T^{-2}] is the effective stress tensor, $\sigma'_m = \left(\sigma'_x + \sigma'_y + \sigma'_z\right)/3$ [M L^{-1} T^{-2}] is the mean effective stress, $\mathbf{I}$ [-] is the identity matrix, $K = E/\left(3\left(1-2\nu\right)\right)$ [M L^{-1} T^{-2}] is the bulk modulus, $G = E/\left(2\left(1+\nu\right)\right)$ [M L^{-1} T^{-2}] is the shear modulus, E [M L^{-1} T^{-2}] is the Young's modulus and ν [-] is Poisson ratio.

We model CO_2 injection at a constant mass flow rate through a vertical well. Due to the symmetry of the problem, the model is axisymmetric. We include in the model the storage formation, the caprock and the baserock (Figure 2). The top of the storage formation is at a depth of 1500 m. We assume isothermal conditions, with a constant temperature of the storage formation equal to 60 ºC, which corresponds to a surface temperature of 10 ºC and a geothermal gradient of 33 ºC/km.

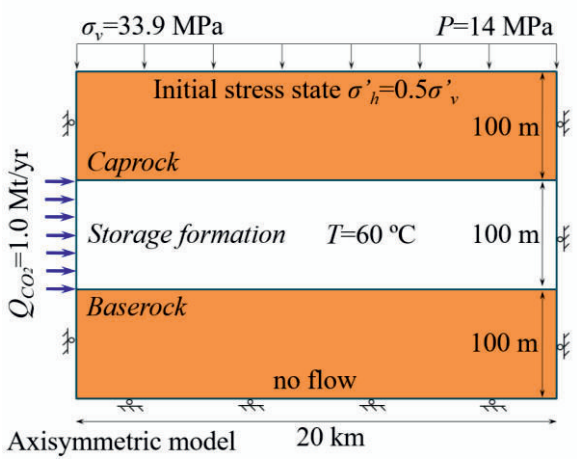

Figure 2. Schematic representation of the numerical model for simulating CO_2 injection in an extensive deep saline formation.

The storage formation is assumed to be a permeable sandstone and the caprock and baserock a low permeable shale. The properties of these rocks are detailed in Table 1. The retention curves of the rocks (Figure 3) follow a van Genuchten model [31]

$$S_{ew} = \frac{S_w - S_{rl}}{S_{ls} - S_{rl}} = \left(1 + \left(\frac{p_c - p_w}{p_0}\right)^{\frac{1}{1-\lambda}}\right)^{\lambda}, \quad (5)$$

where p_0 [M L^{-1} T^{-2}] is the entry pressure, λ [-] is the shape function of the retention curve, S_{ew} [-] is the effective water saturation, S_{rl} [-] is the residual liquid saturation and S_{ls} [-] is the maximum liquid saturation. The relative permeability of the storage formation follows a power law of effective saturation, with a cubic law for water and a power equal to 6 for CO_2, which reproduces the higher multiphase flow interference effects for CO_2 than for water that are usually measured in the laboratory [32] (Figure 4).

Table 1. Material properties of the storage formation, the caprock and baserock.

Property	Storage formation	Caprock and baserock
Permeability, k (m^2)	10^{-13}	10^{-18}
Gas entry pressure, p_0 (MPa)	0.02	5
van Genuchten λ (-)	0.6	0.3
Residual liquid saturation, S_{rl} (-)	0.3	0.4
Maximum liquid saturation, S_{ls} (-)	1.0	1.0
Relative water permeability, k_{rw} (-)	S_{ew}^3	S_{ew}^6
Relative CO_2 permeability, k_{rc} (-)	$\left(1-S_{ew}\right)^6$	$\left(1-S_{ew}\right)^6$
Porosity, φ (-)	0.1	0.01
Young's modulus, E (GPa)	10	5
Poisson ratio, ν (-)	0.3	0.3

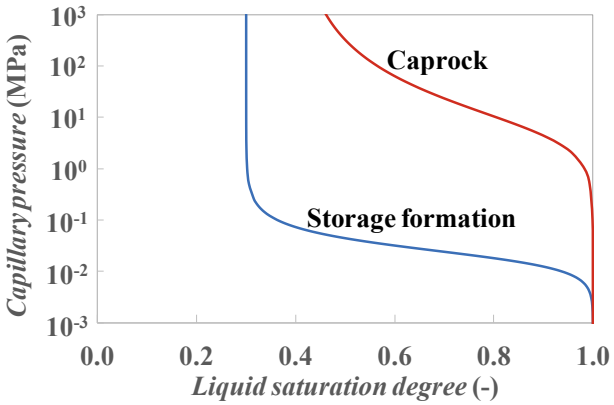

Figure 3. Retention curve of the storage formation and the caprock. The high permeable storage formation is characterized by a low entry pressure and a small slope of the retention curve, indicating that the pores significantly desaturate for small increases in the capillary pressure. In contrast, the low permeable caprock presents a high entry pressure and a high increase in the capillary pressure is needed to desaturate the pores (note the logarithmic scale of the vertical axis).

We inject 1 Mt/yr of CO_2 during 1 year. Since the model extends laterally 20 km, the pressure perturbation cone, which is slightly larger than 10 km after 1 year,

does not reach the outer boundary during the injection time. Thus, the outer boundary condition does not influence the results and the storage formation in our model is an infinitely acting aquifer.

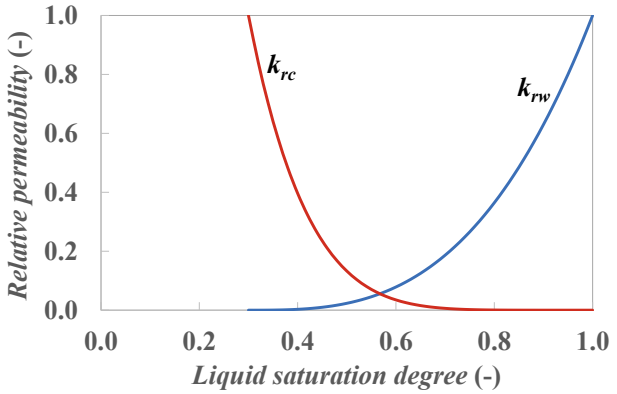

Figure 4. Relative permeability to water and CO_2 of the storage formation.

We simulate CO_2 injection in a deep saline formation using the finite element code CODE_BRIGHT [33, 34], extended for CO_2 injection [25]. CO_2 density is calculated using the cubic Redlich-Kwong equation of state with the parameters proposed for CO_2 by Spycher et al. [6]. CO_2 viscosity is calculated according to the empirical expression developed by Altunin and Sakhabetdinov [35]. The mesh is made of structured quadrilateral elements. Radially, the size of the elements is of a few cm close to the injection well and increases progressively up to 3000 m next to the outer boundary. Vertically, the storage formation is discretized with 5 m thick elements. The element size grows in the caprock and baserock from 5 m at the contact with the storage formation to 25 m far away from it. We performed a mesh sensitivity analysis to ensure that results are not influenced by further refinements.

3 Results

3.1. CO_2 injection pressure evolution

Figure 5 shows the overpressure evolution at the injection well induced by injection of 1 Mt/yr of CO_2. CO_2 injection pressure is characterized by an initial peak followed by a slight decrease in overpressure. The sharp increase at the beginning of injection is caused by the very low relative permeability to CO_2 that occurs as the pores around the injection well start to desaturate (recall Figure 4). Initially, the capillary fringe, where two-phase flow effects are dominant, completely surrounds the injection well (Figure 6a). As long as the capillary fringe surrounds the injection well, the low relative permeability values act as a negative skin effect of the injection well, causing the sharp increase in injection pressure. However, as CO_2 injection continues, the capillary fringe is displaced away from the injection well and CO_2 eventually fills the pores around the injection well, reaching the residual liquid saturation. At this stage, the relative permeability to CO_2 approaches unity and since the viscosity of supercritical CO_2 is one order of magnitude lower than that of brine, CO_2 flows easily through the well-connected pores filled with CO_2 and overpressure starts to drop (Figure 6b). Due to buoyancy, CO_2 tends to migrate upwards and advances preferentially through the top of the storage formation. As the capillary fringe is displaced away from the injection well, the pressure drop that occurs through it progressively decreases (see the magnitude of the arrows in Figure 7). While the retention curve and relative permeability curves have a small effect on the magnitude of the induced overpressure, the retention curve controls the CO_2 distribution within the CO_2 plume and the extent of the CO_2 plume [36]. Overall, overpressure induced by CO_2 injection tends to slightly decrease with time after the initial sharp increase.

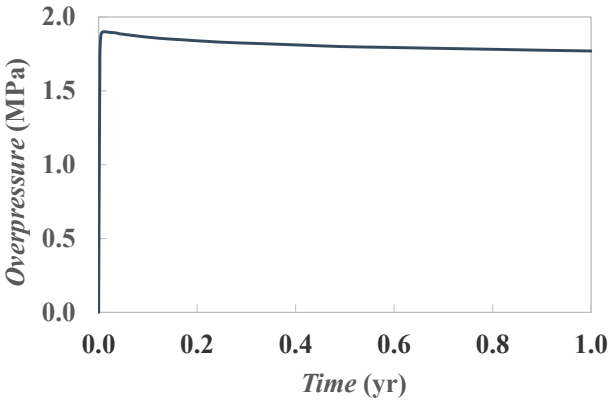

Figure 5. Overpressure evolution as a result of injecting 1 Mt/yr of CO_2.

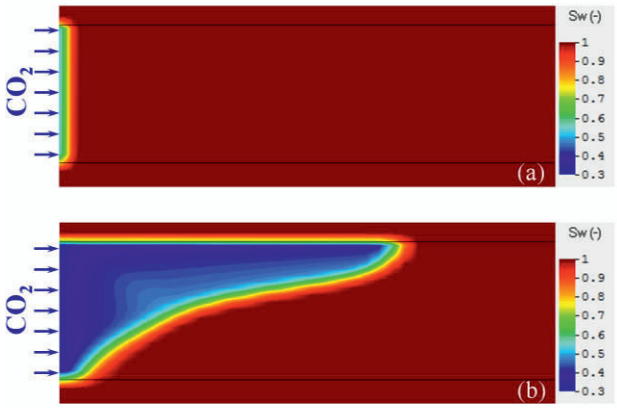

Figure 6. Cross section of an axisymmetric CO_2 plume (a) at the beginning of injection, coinciding with the peak in overpressure caused by the low values of the relative permeability in the capillary fringe and (b) once the CO_2 has filled the pores in the vicinity of the injection well and can flow easily due to its low viscosity, which induces a slight decrease in overpressure as the capillary fringes moves away from the injection well. Note that CO_2 tends to advance preferentially through the top of the storage formation due to buoyancy.

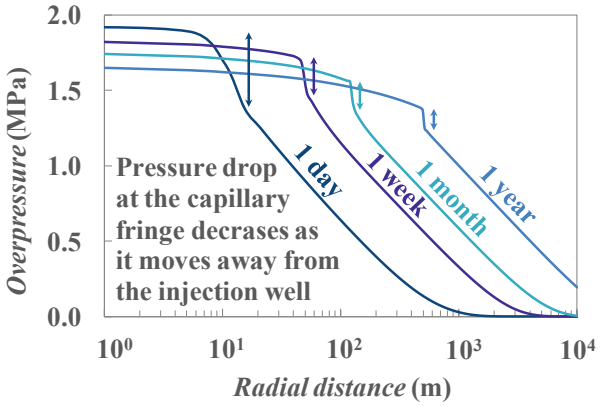

Figure 7. Fluid overpressure at the top of the storage formation as a function of the distance from the injection well for several injection times. Note that the pressure drop at the capillary fringe (indicated with an arrow) decreases as the capillary fringe moves away from the injection well.

3.2 Caprock geomechanical stability

Fluid pressure evolution has a direct effect on the caprock geomechanical stability. Even though the low permeability of the caprock prevents overpressure from propagating quickly into the caprock, the portion of the caprock that is close to the interface with the storage formation undergoes an overpressure similar to that of the storage formation, but delayed. Since overpressure induces a reduction in the effective stresses, the stress state evolves towards failure conditions (Figure 8). The initial sharp increase in injection pressure shifts the Mohr circle towards the failure envelope. However, the horizontal stresses increase in response to overpressure, which causes a decrease in the size of the Mohr circle. As a result, the caprock remains stable, being still some margin before failure conditions are reached. In the long-term, after the peak in overpressure, caprock stability slightly improves as a result of the slight decrease in overpressure. Thus, the most critical situation occurs at the beginning of injection. Consequently, it may be advisable to progressively inject CO_2 at the beginning of injection to avoid inducing a sharp increase in overpressure as the pores around the injection well get filled with CO_2.

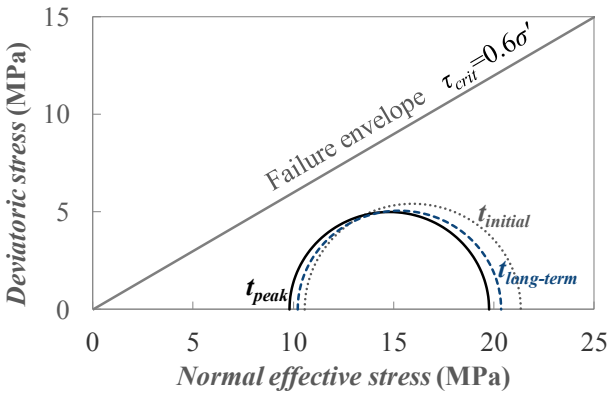

Figure 8. Stability evolution of the lower portion of the caprock next to the injection well as a result of injecting 1 Mt/yr of CO_2.

This overpressure evolution induced by CO_2 injection significantly differs from that generated by water injection. Recently, the feasibility of geologic carbon storage to significantly reduce CO_2 emissions has been put in doubt because it was compared with wastewater disposal [37], which is inducing a large number of large earthquakes (magnitude greater than 4) in the central US [38]. However, the geomechanical response of CO_2 injection will be completely different to that of wastewater disposal, making geological carbon storage a safe option for mitigating climate change [15, 39].

4 Summary and conclusions

CO_2 injection in deep geologic formations implies a two-phase flow in which the relative permeability plays a major role on the fluid pressure evolution. Overpressure induced by CO_2 injection peaks at the beginning of injection caused by the low values of the relative permeability to CO_2 as the pores start to desaturate. However, once the pores surrounding the injection well get filled with CO_2 and the residual liquid saturation is reached, the relative permeability to CO_2 approaches one and since the viscosity of supercritical CO_2 is one order of magnitude lower than that of brine, overpressure reaches a maximum and starts decreasing slightly. Additionally, the pressure drop that occurs in the capillary fringe due to two-phase flow interference decreases as the capillary fringe is displaced away from the injection well. The fact that overpressure does not continuously increase with time is beneficial to maintain the caprock integrity. Thus, the caprock sealing capacity is not altered and CO_2 leakage across the caprock does not take place. The peak in overpressure at the beginning of injection coincides with the least stable situation. To minimize the initial changes on the caprock stability, a good practice would be to progressively inject CO_2, so that the pores around the injection well slowly fill with CO_2 and the peak in injection pressure would be avoided. Overall, CO_2 injection induces an overpressure that can be easily controlled to avoid damaging the caprock or reactivating faults, which makes geologic carbon storage a feasible option to significantly reduce CO_2 emissions to mitigate climate change.

References

1. IEA. *Energy technology perspectives. Scenarios & strategies to 2050. Executive summary*, International Energy Agency (2010).
2. K. Michael, A. Golab, V. Shulakova, J. Ennis-king, G. Allinson, A. Sharma, T. Aiken, Int. J. Greenh. Gas Contr., **4**, 659–667 (2010).
3. J.T. Birkholzer, C. Oldenburg, Q. Zhou, Int. J. Greenh. Gas Contr., **40**, 203–220 (2015).
4. S. Bachu, Environ. Geol., **44**, 277–289 (2003).
5. M.L. Szulczewski, C.W. MacMinn, H.J. Herzog, R. Juanes, Proc. Nat. Acad. Sci., **109**, 5185-5189 (2012).
6. N. Spycher, K. Pruess, J. Ennis-king, Geochimica et Cosmochimica Acta, **67**, 3015–3031 (2003).

7. A. Riaz, M.A. Hesse, H.A. Tchelepi, F.M. Orr, Jr., J. Fluid Mech., **548**, 87–111 (2006).
8. J.J. Hidalgo, J. Carrera, J. Fluid Mech., **640**, 443–454 (2009).
9. G.S.H. Pau, J.B. Bell, K. Pruess, A.S. Almgren, M.J. Lijewski, K. Zhang, Adv. Water Res., **33**, 443–455 (2010).
10. J. Rutqvist, Int. J. Geotech. Geol. Eng., **30**, 525–551 (2012).
11. J.M. Miocic, S. Gilfillan, C. McDermott, R.S. Haszeldine, Energy Procedia, **40**, 320-328 (2013).
12. J.T. Birkholzer, Q. Zhou, C.F. Tsang, Int. J. Greenh. Gas Contr., **3**, 181-194 (2009).
13. F. Cappa, J. Rutqvist, Geophys. Res. Lett., **38**, L17313 (2011).
14. J. Verdon, Environ. Res. Lett., **9**, 064022 (2014).
15. V. Vilarrasa, J. Carrera, Proc. Nat. Acad. Sci., **112**, 5938-5943 (2015).
16. M.O. Häring, U. Schanz, F. Ladner, B.C. Dyer, Geothermics, **37**, 469–95 (2008).
17. S. Cesca, F. Grigoli, S. Heimann, A. Gonzalez, E. Buforn, S. Maghsoudi, E. Blanch, T. Dahm, Geophys. J. Int., **198**, 941-953 (2014).
18. S. Horton, Seismolo. Res. Lett., **83**, 250-260 (2012).
19. S.A. Mathias, P.E. Hardisty, M.R. Trudell, R.W. Zimmerman, Transp. Porous Media, **79**, 265–284 (2009).
20. J.M. Nordbotten, M.A. Celia, S. Bachu, Transp. Porous Media, **58**, 339–360 (2005).
21. V. Vilarrasa, D. Bolster, M. Dentz, S. Olivella, J. Carrera, Transp. Porous Media, **85**, 619–639 (2010).
22. M. Dentz, D.M. Tartakovsky, Transp. Porous Media, **79**, 15–27 (2009).
23. V. Vilarrasa, J. Carrera, D. Bolster, M. Dentz, Transp. Porous Media, **97**, 43-65 (2013).
24. J. Henninges, A. Liebscher, A. Bannach, W. Brandt, S. Hurter, S. Köhler, F. Möller, CO2SINK Group, Energy Procedia, **4**, 6085–6090 (2011).
25. V. Vilarrasa, D. Bolster, S. Olivella, J. Carrera, Int. J. Greenh. Gas Contr., **4**, 910–919 (2010).
26. R.T. Okwen, M.T. Stewart, J.A. Cunningham, Int. J. Greenh. Gas Contr., **5**, 1140-1148 (2011).
27. K.Y. Kim, W.S. Han, J. Oh, T. Kim, J.C. Kim, Transp. Porous Media, **92**, 397-418 (2012).
28. M.J. Martinez, P. Newell, J.E. Bishop, D.Z. Turner, Int. J. Greenh. Gas Contr., **17**, 148-160 (2013).
29. M. Burton, N. Kumar, S.L. Bryant, Energy Procedia, **1**, 3091-3098 (2009).
30. J.Bear, *Dynamics of fluids in porous media* (Elsevier, New York, 1972).
31. R. van Genuchten, Soil Sci. Soc. Am. J., **44**, 892–898 (1980).
32. B. Bennion, S. Bachu, SPE Reserv. Eval. Eng., 11, 487–96 (2008).
33. S. Olivella, J. Carrera, A. Gens, E.E. Alonso, Transp. Porous Media, **15**, 271–293 (1994).
34. S. Olivella, A. Gens, J. Carrera, E.E. Alonso, Eng. Computations, **13**, 87–112 (1996).
35. V.V. Altunin, M.A. Sakhabetdinov, Teploenergetika, **8**, 85–89 (1972).
36. V. Vilarrasa, J. Rutqvist, A.P. Rinaldi, Greenhouse Gases: Sci. & Tech., **5**, 449-461 (2015).
37. M.D. Zoback, S.M. Gorelick, Proc. Nat. Acad. Sci., **109**, 10164–10168 (2012).
38. W.L. Ellsworth, Science, **341**, 1225942 (2013).
39. V. Vilarrasa, J. Carrera, Proc. Nat. Acad. Sci., **112**, E4511-E4511 (2015).